Frontiers in Health InformaticsISSN-Online: 2676-7104
www.healthinformaticsjournal.com
2025; Vol 14: Issue 2
Open Access

# A Predictive Control Model Based on Environmental Parameter Modeling (Temperature and Humidity) for HVAC Systems to Enhance Thermal Comfort and Reduce Energy Consumption

**Mohsen Akhlaghi Ketabi[1], Mohammad Reza Aligoodarz[2]**

[1]Engineering, Power Conversion, Shahid Rajaee Teacher Training University, Tehran, Iran
[2]Associate Professor, Department of Fluid Mechanics, Faculty of Mechanical Engineering, Shahid Rajaee Teacher Training University (SRU), Tehran, Iran
*Corresponding Author

Cite this paper as: Mohsen Akhlaghi Ketabi, Mohammad Reza Aligoodarz (2025), A Predictive Control Model Based on Environmental Parameter Modeling (Temperature and Humidity) for HVAC Systems to Enhance Thermal Comfort and Reduce Energy Consumption. *Frontiers in Health Informatics*, *14(2) 3211-3231*

**ABSTRACT**

This study proposes a predictive control model for HVAC systems based on the modeling of environmental parameters, such as temperature and humidity, to improve thermal comfort and reduce energy consumption. This research is a modeling-based study that employs MATLAB software along with a metaheuristic algorithm. To evaluate and compare the methods, two metrics—RMSE and $R^2$—were used. Both the MLP (Multi-Layer Perceptron) method and the Genetic Algorithm were applied to assess their accuracy as effective approaches for time-series prediction.

The results indicate that, in terms of $R^2$, the Genetic Algorithm's performance in predicting room temperature and humidity affected by the HVAC system is comparable to that of the MLP method. Overall, the MLP network demonstrated the highest prediction accuracy. The Genetic Algorithm, however, showed lower accuracy for humidity prediction. To investigate this further, the accuracy of the MLP model was evaluated without disrupting the data sequence. In this case, the $R^2$ value was 0.559, and the RMSE was 0.12. The notable reduction in $R^2$ compared to when the data sequence was preserved in the MLP network, along with the low $R^2$ of the Genetic Algorithm, highlights its limitations for this application.

**Key words:** Predictive control model, uncertainty, HVAC systems, Genetic Algorithm.

## INTRODUCTION

The depletion of energy resources, such as fossil fuels and nuclear energy, has highlighted the need for strategies aimed at reducing energy consumption. Residential buildings, as a significant part of the non-industrial sector, present an accessible opportunity for energy savings [1]. Energy use in these buildings can be substantially decreased through behavioral modifications, load scheduling, demand-side management, and other similar strategies [2]. Building automation systems play a critical role in scheduling loads and shifting energy consumption from peak to off-peak hours; however, such shifts may compromise occupants' thermal comfort [3]. Therefore, implementing an effective controller to maximize energy savings is essential.

With rising living standards, the number of air-conditioning users is projected to grow exponentially in the coming years. Consequently, energy consumption in buildings—particularly for heating and cooling—is expected to increase rapidly and continuously. In light of this trend, optimizing energy efficiency in HVAC systems becomes increasingly important. Energy savings can be achieved by reducing cooling demand through improved air-conditioning systems or by controlling system operations more effectively.

Historically, research has focused on optimizing building design, employing insulation materials, and utilizing energy storage systems to reduce building energy consumption. More recent studies, however, emphasize the development of control strategies aimed at minimizing energy consumption based on analyses of users' energy consumption patterns.

For example, Aghileh et al. [4] (2019) investigated the impact of different construction materials on energy consumption and applied fuzzy control to HVAC systems to maintain thermal comfort while reducing energy use. Their study involved creating building energy models and validating them using utility bills. Fuzzy controllers were then employed to evaluate energy consumption while maintaining occupant comfort and indoor air quality. Gholamzadeh et al. [5] (2020) examined advanced control strategies and their impact on energy savings in buildings and HVAC systems. These strategies are responsive to environmental conditions and user behavior. While predictive control models are widely used, they are less effective for systems with high uncertainty or unpredictable inputs. To overcome these limitations, adaptive predictive control strategies—combining predictive and adaptive control—have been developed. Karli et al. [6] (2020) proposed an IoT-based architecture for implementing predictive control in real-world HVAC systems. The MPC algorithm ensures real-time thermal comfort and energy management. In this IoT framework, control and actuation are internet-connected, and a remote interface allows end-users to interact with the HVAC system.

Limperopoulos et al. [7] (2020) introduced a distributed adaptive control strategy for multi-zone HVAC systems. This method effectively regulates zone temperatures through online learning and information exchange among neighboring zones. Each local controller compensates for the influence of adjacent zones and potential variations in system parameters. Real-time estimation of interconnection parameters, combined with exchanged data, enables more precise local temperature control. Esrafilian et al. [8] (2021) focused on minimizing HVAC energy consumption while maintaining acceptable thermal comfort and indoor air quality. An adaptive post-event control strategy was implemented to optimize system performance; however, uncertainties in the system were not fully modeled. Results from implementation in a smart building demonstrated significant potential energy savings using this control approach. Taheri et al. [9] (2022) proposed a predictive control model for HVAC systems that integrates modeling techniques with optimization algorithms. The study analyzed various design aspects—including prediction horizon and building type—to evaluate their impact on control performance. Technical features, advantages, and limitations were discussed, and the results confirmed the effectiveness of this predictive control approach for HVAC system management.

Nadim et al. [10] (2022) investigated the design of HVAC systems for workshop buildings in hot and humid climates using the Cooling Load Temperature Difference (CLTD) method and Hourly Analysis Program (HAP) software. Two approaches were employed in their study: the CLTD method and the HAP software analysis. The cooling load calculated using the CLTD method was 190.7 kW, equivalent to 54.25 tons of refrigeration (TR), while the cooling load estimated using HAP was 195.2 kW, equivalent to 55.5 TR. Bahara et al. [11] (2023) proposed a predictive control model for inverter-based air-conditioning systems. Their findings indicated that both conventional predictive control and adaptive predictive control could maintain thermal comfort within the desired range throughout the day. However, the adaptive predictive control model achieved over 7% energy savings compared to the conventional predictive control approach. Sunfam et al. [12] (2023) studied HVAC optimization in buildings using a combination of the Grey Wolf Optimizer (GWO) and Artificial Neural Networks (ANN). The considered system integrated Variable Air Volume (VAV) system with a Dedicated Outdoor Air System (DOAS). Several factors, including thermostat settings, passive solar design, and cooling system control, were treated as decision variables. The predicted percentage of dissatisfied occupants (PPD) and annual building energy consumption were selected as objective

functions, and multi-objective optimization was applied to optimize system performance.

Fadel [13] (2023) focused on the robust modeling and optimization of commercial air-water HVAC systems. Air-water systems, commonly used in offices and hotels where precise temperature control is required, have received limited research attention. This study proposed a convex modeling approach and demonstrated that thermal comfort could be maintained while accounting for modeling approximations and system uncertainties. Zhao et al. [14] (2023) carried out an experimental study on a data-driven online energy management framework for HVAC systems. Their results showed average reductions of 4.9%, 30.2%, 49.3%, and 73.9% in energy use under specific operational conditions. The proposed framework effectively utilized internal and external heat sources to maintain comfortable indoor temperatures without activating the HVAC system unnecessarily. Pendai et al. [15] (2021) examined a model predictive thermal comfort controller for residential split air-conditioning units. Simulation results demonstrated that the proposed control technique reduced cooling energy consumption by 8.8% to 17.5% compared to baseline cases.

HVAC systems are crucial in reducing building energy consumption; therefore, developing efficient and cost-effective control strategies to maximize energy savings is essential. Conventional control techniques often cannot adequately address system constraints, highlighting the importance of predictive control models for HVAC systems. Additionally, due to uncertainties in weather patterns, modeling uncertain parameters using point estimation methods is critical. Optimizing predictive control performance further requires determining optimal parameter values through optimization algorithms.

Since conventional control methods struggle to handle system constraints and environmental uncertainties, predictive control strategies equipped with adaptive capabilities are necessary to manage stochastic conditions and uncertain weather patterns. Accordingly, this study proposes a predictive control model for HVAC systems aimed at improving energy efficiency, with system uncertainties modeled using a point estimation approach.

## Research Methodology

This study is a modeling-based investigation that utilizes MATLAB software alongside a metaheuristic algorithm. MATLAB was employed to analyze and identify the appropriate model for the time series. The procedure began with a preliminary identification of the time-series pattern based on the autocorrelation and partial autocorrelation function plots. The selected model was then fitted to the data, and residuals—calculated as the difference between the actual and predicted values—were examined by plotting their autocorrelation and partial autocorrelation functions. If the fitted model is appropriate, the residuals' autocorrelation and partial autocorrelation values should be near zero and within the critical limits of $\pm 2/\sqrt{N}$, indicating that the residuals are random and that the model adequately represents the data. In this study, MATLAB was used to plot the autocorrelation and partial autocorrelation functions for the room humidity time series.

To evaluate and compare the predictive methods, two metrics were used: RMSE and $R^2$. RMSE (Root Mean Square Error) provides an average measure of prediction error. It remains small when most errors are minor and only a few are large.

Two predictive approaches were employed: the Multi-Layer Perceptron (MLP) and the Genetic Algorithm, to assess the accuracy of forecasting for time series data. Based on the obtained $R^2$ values, the Genetic Algorithm's performance in predicting room temperature and humidity under HVAC operation was comparable to that of the MLP method.

### Validation of the Simulated System

For validation, the predicted mean air temperature and cooling electricity consumption from the EnergyPlus TS house model were compared with experimental measurements. The EnergyPlus model parameters were calibrated through multiple trial simulations as follows:

1. The HVAC variable refrigerant flow (VRF) system capacity was fixed at 3.5 kW.
2. The supply and return refrigerant pipe lengths were manually set to 1 meter.
3. The internal terminal air flow rate in the EnergyPlus model was set to 0.01 $m^3/s$.
4. To account for shading effects from trees and neighboring buildings, shading elements were positioned approximately at their actual distances.

Because room air temperature measurements are inherently variable, the average of three data points was used to produce a more uniform dataset. The RMSE between the estimated and measured room air temperature was 0.13°C, and the RMSE between the predicted and measured cooling energy consumption was 0.01 kWh. Additionally, the validated EnergyPlus model was used to generate the input/output data necessary for developing a data-driven state-space model of the TS house.

The N4SID algorithm (Numerical Subspace State-Space Identification) from MATLAB's System Identification Toolbox was used to estimate a discrete-time state-space model based on the EnergyPlus input/output data. The identified model was a 9th-order state-space representation, which can be expressed as follows:

$$x(k+1) = Ax(k) + Bu(k) + Hd(k)$$
$$y(k) = Cx(k)$$

**Predictive Model**

Model Predictive Control (MPC) is a control strategy that optimizes control actions over a finite time horizon, known as the prediction horizon, by forecasting future disturbances in the system and avoiding violations of future constraints. The predictive capability of MPC arises from a mathematical model, which is typically derived from system input-output data or the system's physical equations. The objective function used in this study (Equation below) minimizes the error between the predicted mean air temperature and the reference temperature.

$$\min_{\{u(k|k),\, u(k+1|k),\ldots,u(k+q-1|k)\}} \sum_{i=1}^{p} \left(y(k+i|k) - r(k+i|k)\right)^2$$
$$\textit{Subject to}$$
$$x(k+i+1) = Ax(k+i|n) + Bu(k+i|k) + Hd(k|k)$$
$$y(k+i+1|k) = Cx(k+i+1|k)$$
$$i = 1, 2, \ldots, p$$
$$u(k+q|k) = \ldots = u(k+p-1|k) = u(k+q-1|k)$$
$$u_L \leq u(k+i|k) \leq u_H \textit{ for } i = 0, 1, \ldots, q-1$$
$$y_L \leq y(k+i|k) \leq y_H \textit{ for } i = 1, \ldots, p$$

Environmental variables—such as outdoor dry-bulb temperature, wind speed, direct solar radiation, solar radiation transmitted through north- and south-facing windows, and internal heat gains—act as model disturbances. Constraints are applied to the AC setpoint, and the controlled variable is measured, specifically the average air temperature of the master bedroom. At the kth sampling instant, the MPC problem is

formulated as a constrained optimization problem.

The MPC framework in this study consists of three main components:

- The EnergyPlus model of the TS house.
- The "MPC Controller" block in MATLAB, which implements the designed MPC controller.
- A real-time thermal comfort calculation model, which determines the reference temperature for the MPC controller.

## Findings

The Kaiser-Meyer-Olkin (KMO) measure was calculated as 0.78, confirming the suitability of the data for Principal Component Analysis (PCA). Applying PCA to the time series of ten parameters resulted in ten components, with the first component explaining the largest variance and the last component explaining the smallest. Selecting the first few components, which account for the majority of the variance and are considered the principal components, is a critical step in PCA; therefore, careful attention must be paid when determining the threshold for component retention.

Using Varimax rotation on the principal component coefficient matrix, the eigenvectors, which serve as the loadings of each factor in forming the corresponding component, were obtained. The eigenvalues and the variance explained by each component were analyzed after performing the rotation on the PCA-derived component coefficients. Since the first four components were selected as the principal components, the rotation was applied among these four. By rotating the components, the coefficients of each parameter (eigenvectors) were derived to define the components, as presented in Table 1.

**Table 1:** Eigenvector values in Principal Factor Analysis

| Parameters | component | | | |
|---|---|---|---|---|
| | 1 | 2 | 3 | 4 |
| Pressure | .439 | -.051 | -.068 | .852 |
| Humidity | -.207 | -.893 | -.009 | -.006 |
| Temperature | -.098 | .926 | .026 | -.172 |
| Wind Direction | -.224 | -.029 | .897 | .017 |
| Wind Speed | -.278 | .197 | .847 | -.095 |

### Time Series Analysis and Prediction of Temperature and Humidity

In examining the humidity time series, the data exhibited a 24-hour periodicity. Therefore, it can be approximated that the preceding 24 observations may effectively contribute to predictions. Accordingly, an autoregressive (AR) model of order 24 was first fitted to the data using SAS software. By analyzing the autocorrelation and partial autocorrelation functions of the residuals, it was determined that the fitted model was reasonably appropriate.

### Prediction of Temperature and Humidity Using Neural Networks

Temperature and humidity were predicted one step ahead using Multi-Layer Perceptron (MLP) networks and Genetic Algorithm-based networks. The input data for the neural network modeling included components derived from Principal Component Analysis (PCA) applied to the time-lagged series of variables affecting the temperature and humidity prediction system. From the available dataset, 75% of the data were allocated

for network training to determine the network weights, while the remaining 25% were reserved for testing the network's predictive capability after training.

1. **MLP Networks**

MLP networks with various numbers of neurons and layers were implemented, and their predictive accuracies for temperature were analyzed. The optimal architecture was selected as a network with 15 neurons in the hidden layer. The network training function was trainlm, the input layer transfer function was tansig, and the hidden layer transfer function was purelin. The results of the training phase and the corresponding prediction errors are shown in Figure 1. The network was trained over 30 iterations, achieving a mean squared error (MSE) of 0.00242 during training. The results of the testing phase and the prediction errors during testing are presented in Figure 2.

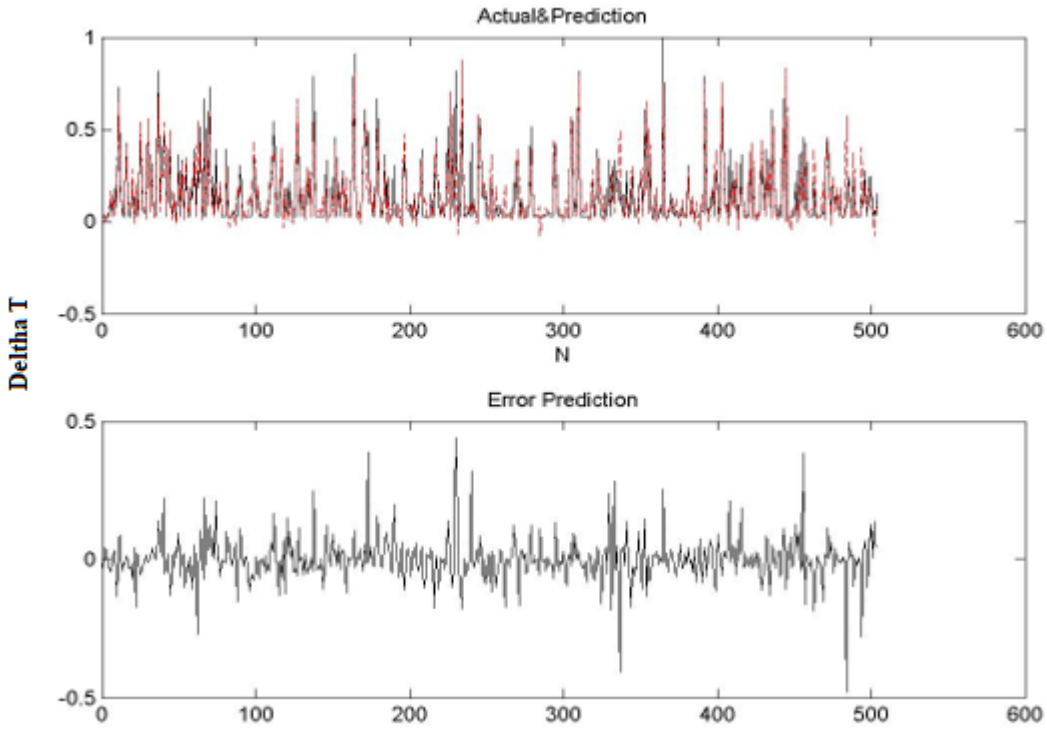


**Figure 1:** Predicted temperature and associated error during the MLP network training phase

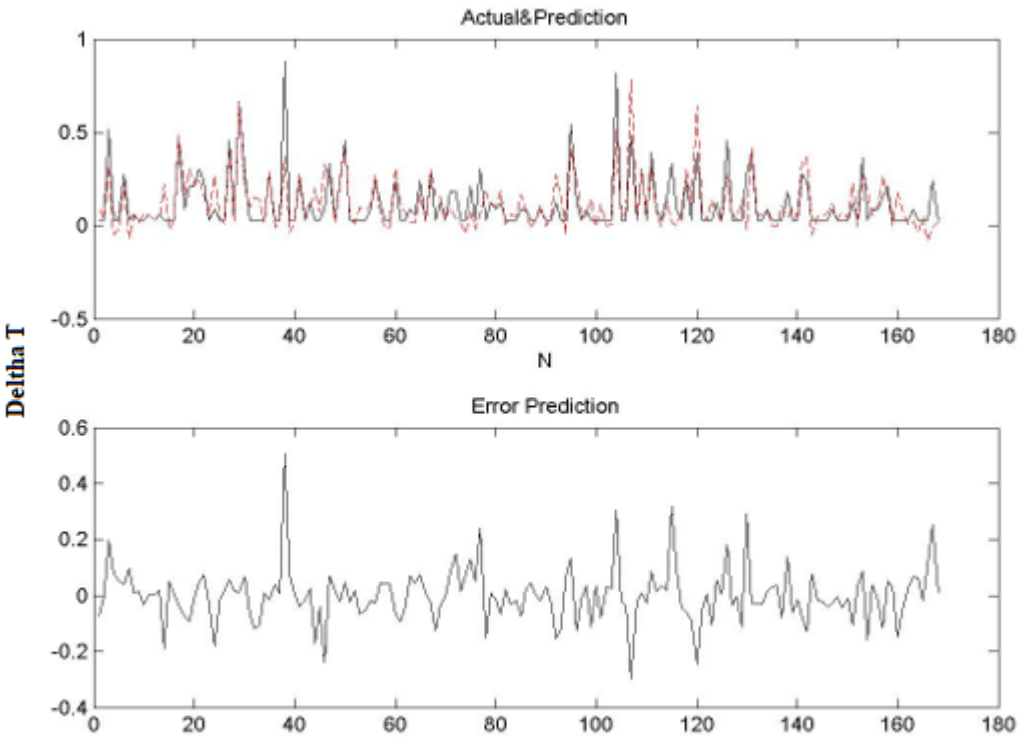


**Figure 2:** Predicted temperature and associated error during the MLP network testing phase

**Figure 3** illustrates the correlation between the actual and predicted data. As shown, the coefficient of determination ($R^2$) between the actual and predicted values is 0.6045. The RMSE for the testing phase was calculated as 0.1.

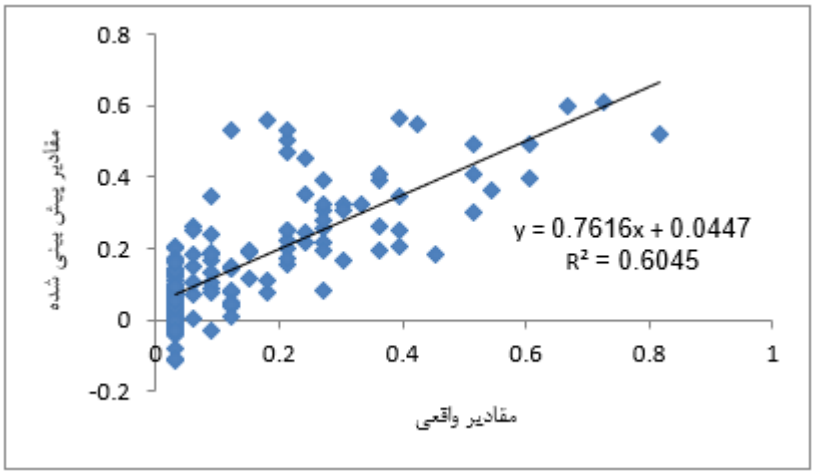


**Figure 3:** Correlation between actual and predicted temperature data in the MLP network

**Table 2:** Error variations for different temperature values

| Error Variations | Temperature Variation Values |
|---|---|
| ±0.094 | 0-0.2 |
| ±0.084 | 0.2-0.4 |

Error variations can be calculated for different temperature ranges by averaging the errors within each range. The computed values are presented in Table 2. For the range 0–0.4, the error can be considered approximately ±0.1.

For predicting humidity, MLP networks with various numbers of neurons and layers were tested. Based on the achieved prediction accuracies, the optimal architecture was selected as a network with 16 neurons in the hidden layer. The results of the training phase and the corresponding prediction errors are shown in Figure 4. The network was trained over 30 iterations, with a mean squared error (MSE) of 0.00309 during training. The results of the testing phase and the prediction errors are presented in Figure 5.

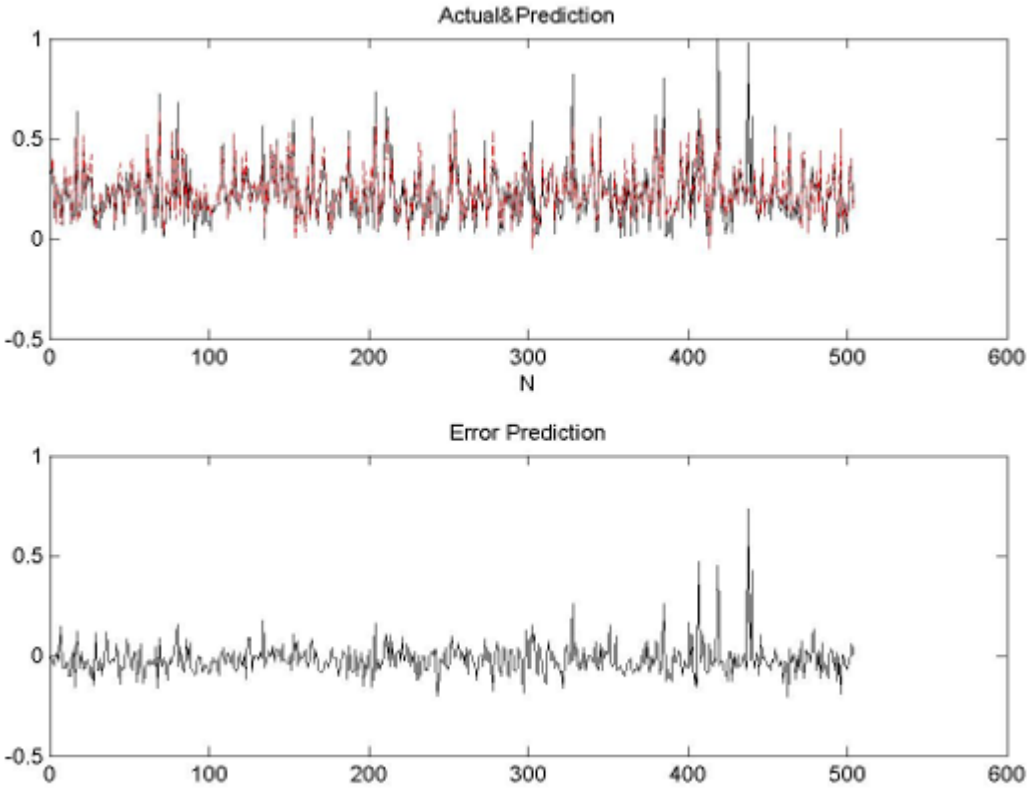


**Figure 4:** Predicted humidity and associated error during the MLP network training phase

**Figure 5** illustrates the correlation between the actual and predicted humidity data. As shown, the coefficient of determination ($R^2$) between the actual and predicted values is 0.6307. The RMSE for the testing phase was calculated as 0.1.

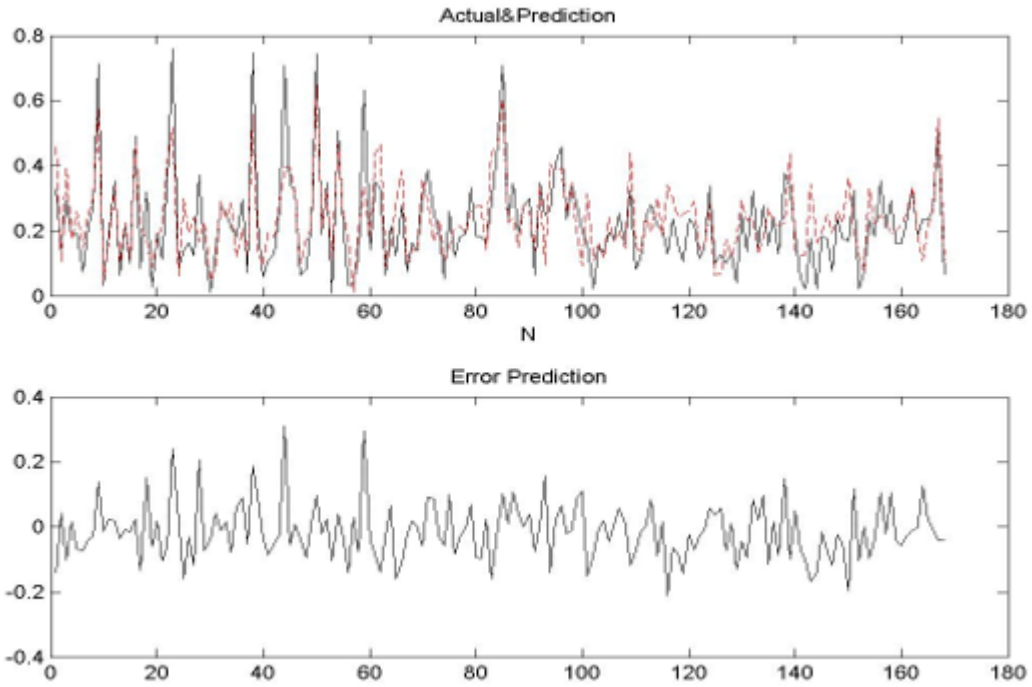


**Figure 5:** Predicted humidity and associated error during the MLP network testing phase

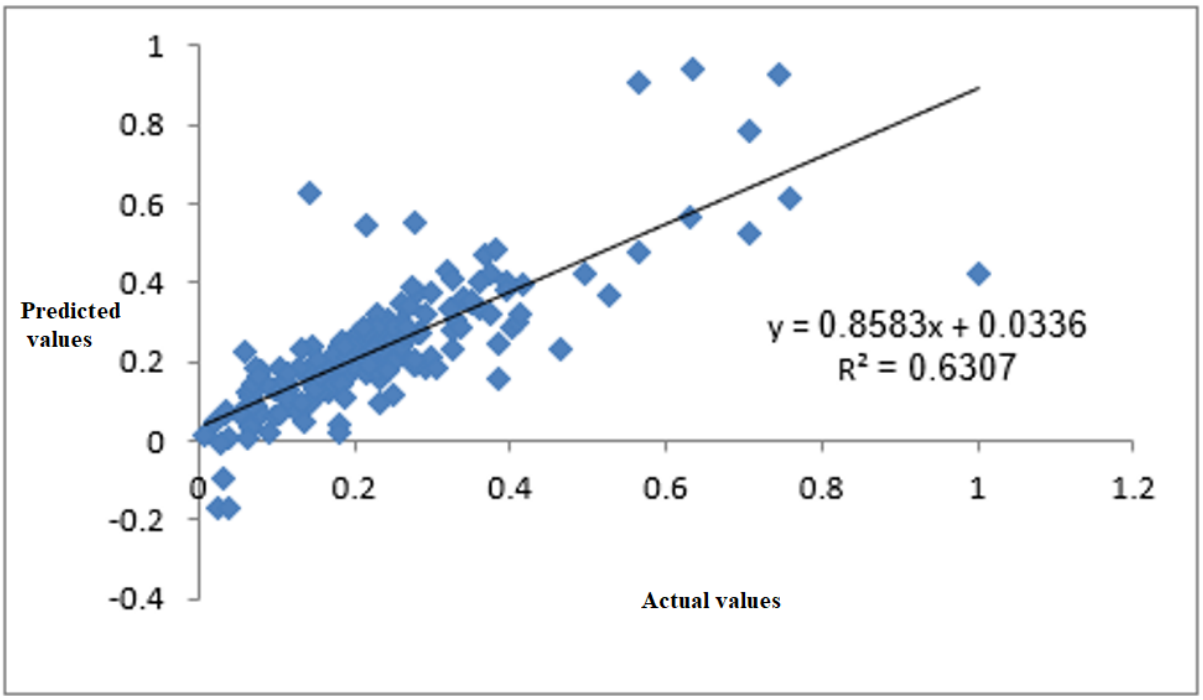


**Figure 6:** Correlation between actual and predicted humidity data in the MLP network

**Table 3:** Error variations for different humidity values

| Error Variations | Humidity Values |
|---|---|
| ±0.072 | 0-0.2 |

| | |
|---|---|
| ±0.087 | 0.2-0.4 |

Error variations for different humidity ranges were obtained by averaging the errors within each range, with the calculated values presented in Table 3. The averaging for these two ranges was performed due to the high frequency of data within them. Based on the computed values, the error in the 0–0.4 range can be considered approximately ±0.08.

**2. Optimization Using the Genetic Algorithm**

Figure 7 shows the room temperature output plots corresponding to 1°C changes in temperature, considering different sampling times and varying numbers of system geometry divisions for comparison purposes.

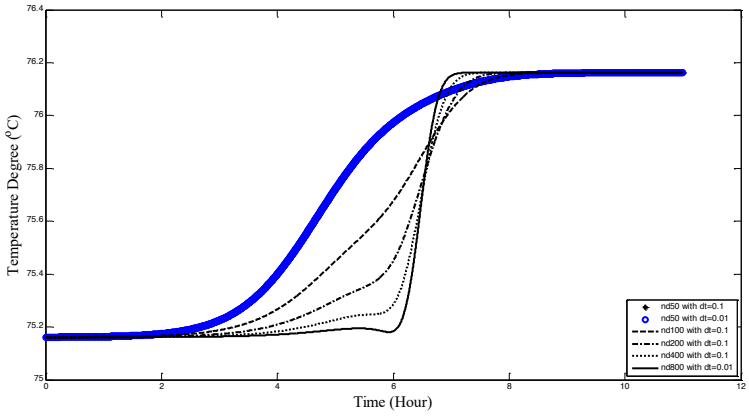


**Figure 7:** Comparison of room temperature output plots for different sampling times and system geometry divisions

In the present study, after programming the main dynamic model of the system and obtaining the room temperature output plots corresponding to 1°C variations from the initial room temperature $T_0$=40°C, the step response was approximated using first- to fourth-order transfer functions. The approximation was performed by minimizing the area between the original curve and the approximated curve. As expected, increasing the system order leads to a higher number of degrees of freedom and greater system complexity. It can also be shown that as the order of the approximated system increases—that is, as the number of system degrees of freedom increases—the value of the above criterion generally decreases. This criterion is minimized at the third-order transfer function approximation. Therefore, selecting a third-order approximated transfer function is considered acceptable. Accordingly, Equations (1) to (4) represent the minimum approximation of the transfer functions at different orders, showing the difference in the area under the curve compared to the original system. The unit step responses of each approximated system are presented in Figures 8 to 11.

$$G_1 = \frac{e^{-6.19s}}{0.324s+1} \Rightarrow ABC = 0.2339 \quad (1)$$

$$G_2 = \frac{e^{-6.95s}}{0.099s^2+0.522s+1} \Rightarrow ABC = 0.1823 \quad (2)$$

$$G_3 = \frac{e^{-5.756s}}{0.028s^3+0.2s^2+0.713s+1} \Rightarrow ABC = 0.1652 \quad (3)$$

$$G_4 = \frac{e^{-4.379s}}{0.321s^4 + 0.814s^3 + 1.85s^2 + 1.955s + 1} \Rightarrow ABC = 0.324 \quad (4)$$

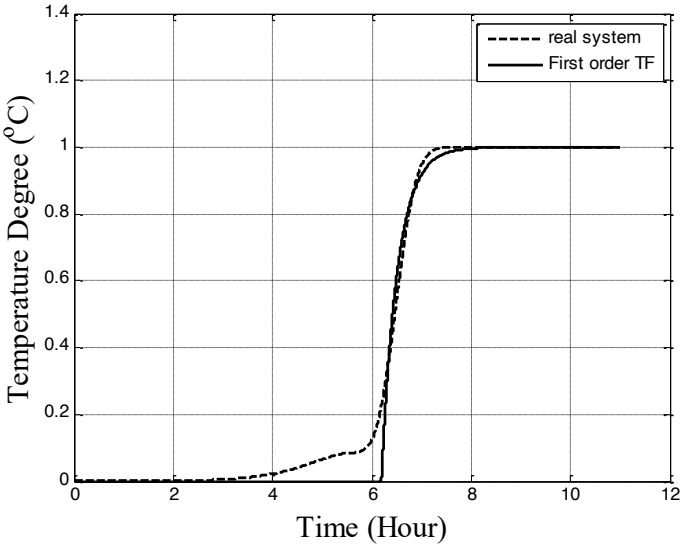


Figure 8: Step response of the approximated first-order transfer function.

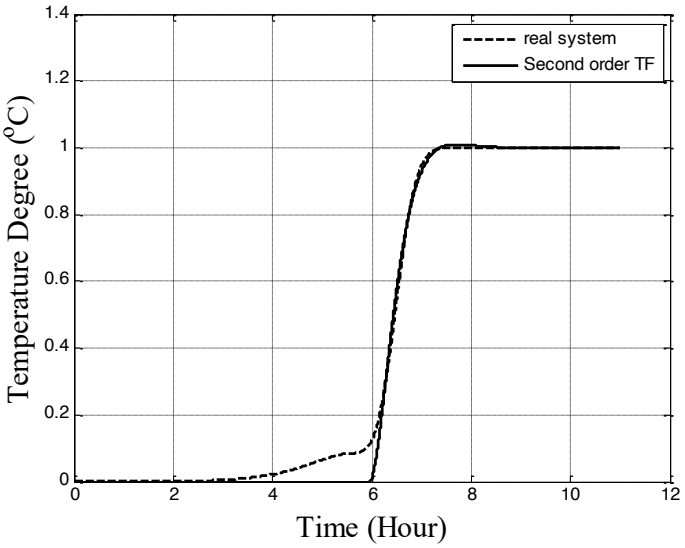


Figure 9: Step response of the approximated second-order transfer function.

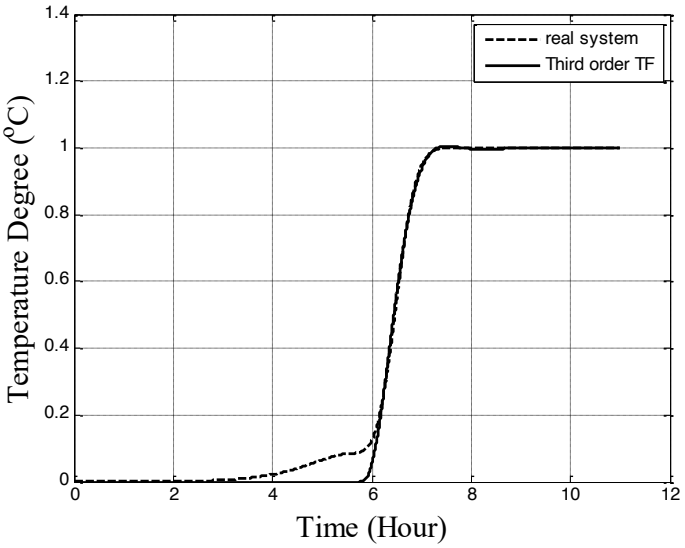


Figure 10: Step response of the approximated third-order transfer function.

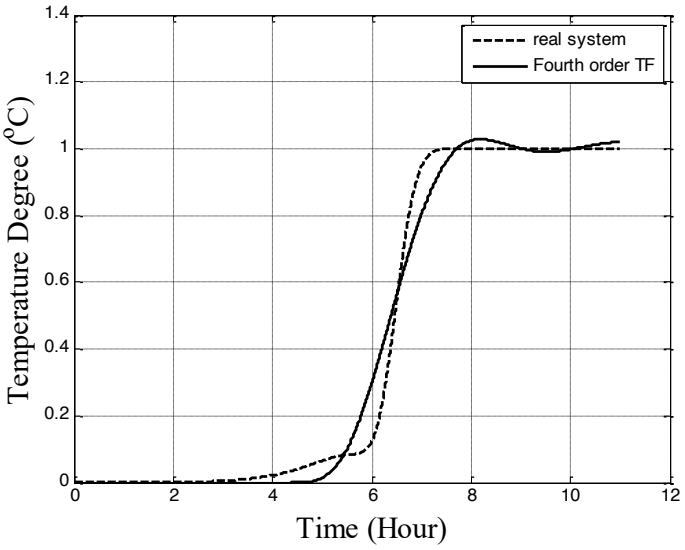


Figure 11: Step response of the approximated fourth-order transfer function.

By carefully examining the room temperature output curve in the original system, corresponding to an increase of one degree Celsius from an initial room temperature of $T_0$=40°C, it can be concluded that Figure 11 may also represent the sum of two first-order transfer functions with dead time. Therefore, according to the above relationships, an attempt was made to fit the sum of two first-order transfer functions with dead time based on Equation (5). The step response of this sum of the two first-order transfer functions is also presented in Figure 12 for comparison.

$$G = G_1 + G_2 = \frac{0.1068e^{-3.9447s}}{1.0188s+1} + \frac{0.8952e^{-6.2526s}}{0.2991s+1} \Rightarrow ABC = 0.0939 \quad (5)$$

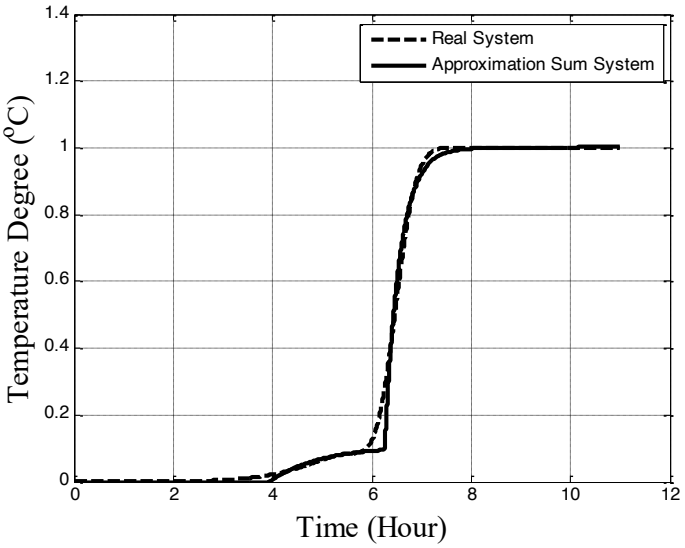


Figure 12: Step response of the sum of two first-order transfer functions with dead time.

Thus, it can be concluded that among all the approximated transfer functions presented above, the transfer function in Equation (5), according to the criterion in Equation (1), can be considered the best choice for selecting the transfer function under study for controller design. Now, after the final selection of the transfer function in Equation (5) as the transfer function under study—which has been approximated with a time step of 0.1 and 400 divisions—this transfer function is examined to become familiar with its characteristics.

As observed in Equation (5), this transfer function consists of two parts in the form of the sum of two transfer functions with dead times. Before further analysis, each of the dead times of the two transfer functions is first approximated using a first-order Padé approximation, as expressed in Equation (6).

$$G = G_1 + G_2 = \frac{0.1068}{1.0188s+1} \times \frac{1-\frac{3.9447}{2}s}{1+\frac{3.9447}{2}s} + \frac{0.8952}{0.2991s+1} \times \frac{1-\frac{6.2526}{2}s}{1+\frac{6.2526}{2}s} \quad (6)$$

As shown in Equation (6), the system has two real minimum-phase zeros at −1.0987and 0.4703, as well as one real non-minimum-phase zero at 0.3329. By examining Equation (6), it can be seen that the system has four real minimum-phase poles at −3.3434, −0.9815, −0.5070, and −0.3197. Figures 13, 14, and 15 respectively show the Bode plot, the Nyquist plot, and the root locus of the system.

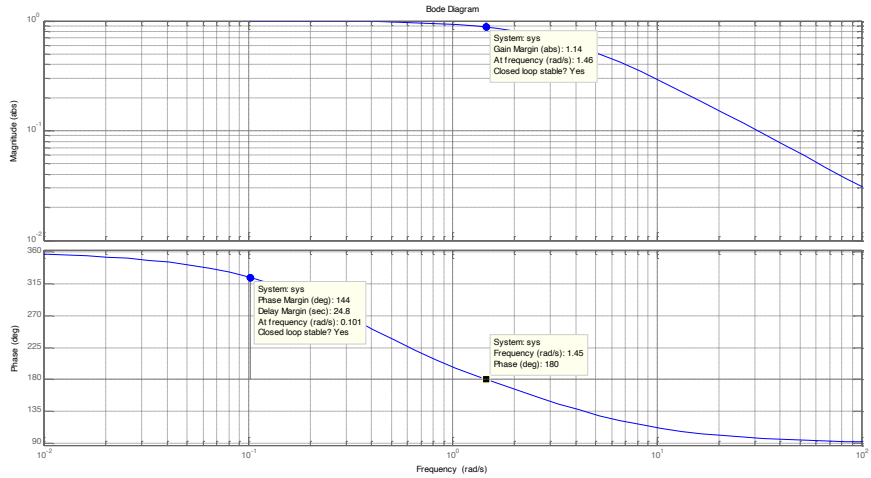


Figure 13: Bode plot of the sum of two first-order transfer functions.

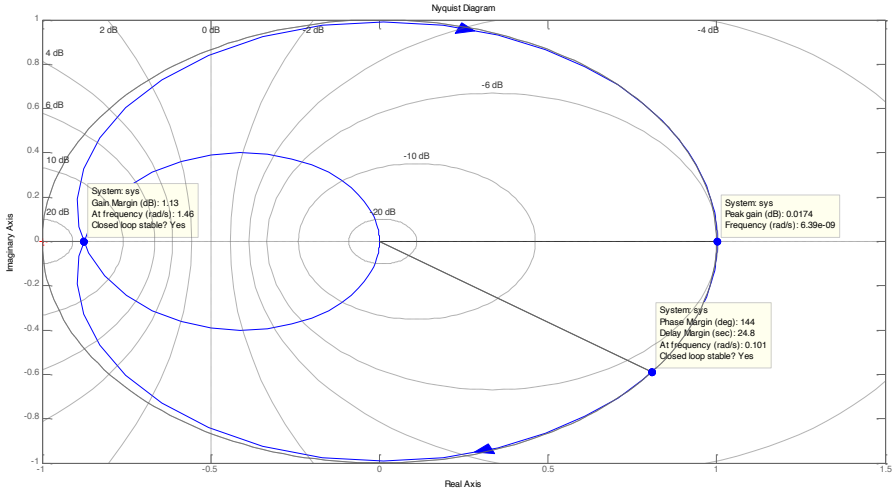


Figure 14: Nyquist plot of the sum of two first-order transfer functions.

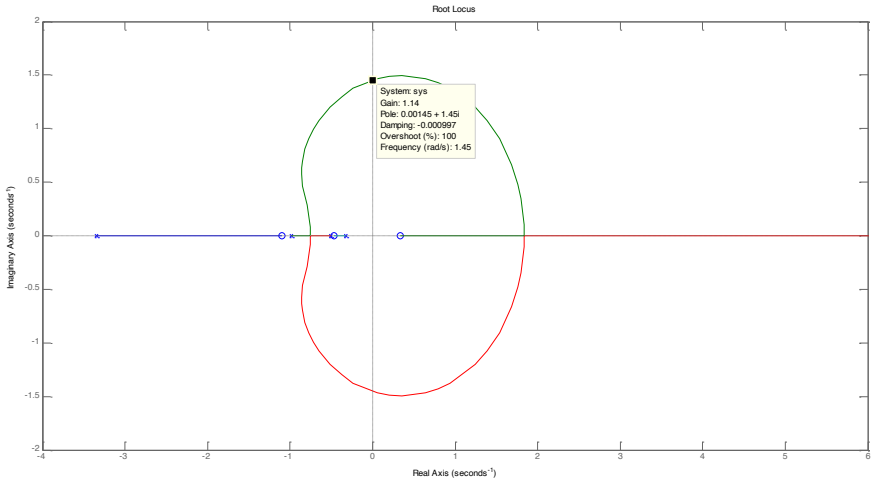


Figure 15: Root locus of the system formed by the sum of two first-order transfer functions.

As observed in Figure 16, if a one-unit change is applied to the system input temperature—that is, if a unit step input is applied to the system—it can be concluded that optimal conditions can be achieved solely by adjusting the system temperature and applying the input to the room temperature transfer function obtained in Equation (5).

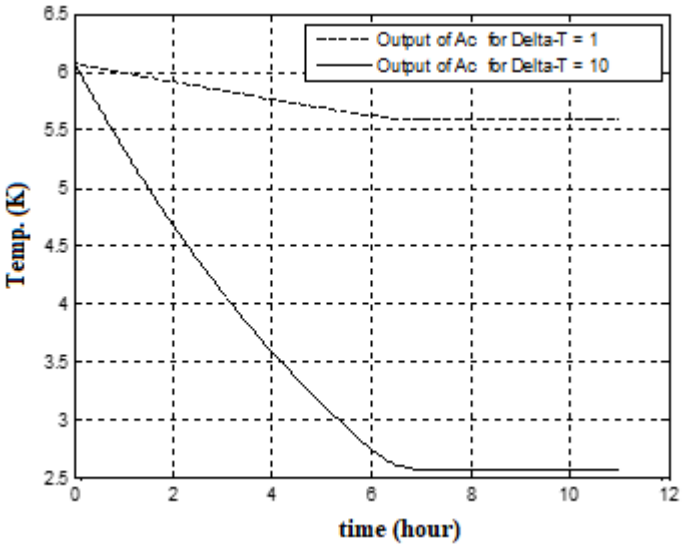


Figure 16: Comparison of room temperature output for different temperature variation inputs.

**MPC Simulation**

The energy storage system is a key component for all microgrids because it allows the intermittent power from RES to be smoothed and helps reduce peak load. Its main benefit is that it effectively manages the balance between supply and demand over a 24-hour period. In the context of microgrids, the energy storage system acts as a backup when the total generated power cannot fully meet the load demand.

Therefore, let $E_i(k)$ be the energy stored in the i-th battery at time k, and $P_i^b(k)$ be the electrical power exchanged with the storage. Then, the dynamics of the storage capacities can be modeled as follows:

(7) $E_i(k+1) = E_i(k) + \eta_i P_i^b(k)$

(8) $\underline{E} \le \underline{E_i(K)} \le \overline{E}$

Which $\eta_i = \begin{cases} \eta^{ch}, & P_i^b(k) > 0 \\ 1/\eta^{dch}, & otherwise \end{cases}$

Typically, $\eta_i$ represents the efficiency of the charge/discharge process, where $\eta^{ch}$ is the charging efficiency and $\eta^{dch}$ is the discharging efficiency, with $0 < \eta^{ch}, \eta^{dch} < 1$ و $\underline{E}$ $\overline{E}$ denote the minimum and maximum allowable stored energy in the battery, respectively.

A cost function is considered to account for battery wear, with deep discharge being the primary concern. The battery cost is modeled as follows:

(9) $C_b(P_i^b) \triangleq \sum_{k=1}^{\infty}(\min(E_i(k) - \alpha_b \overline{E}, 0))^2$

where $\alpha_b$ is a positive constant, representing a discharge penalty when the energy stored in the battery, $E_i(k)$, falls below the maximum battery capacity, $E^-$.

2. **Load Modeling:** We consider interruptible loads as a type of controllable load. For an interruptible load, the consumed energy is constrained as follows:

(10) $\underline{P_i^L} \le P_i^L(K) \le \overline{P}_i^L$

where $P_i^L$ and $P^-_i{}^L$ are the minimum and maximum active power, respectively.

For each electrical load, a cost function measures customer dissatisfaction based on the scheduling of the demand $P_i^L(k)$. The cost function for an interruptible load can be defined as follows:

(11) $C_l(P_i^L) \triangleq \sum_{k=1}^{\infty} \alpha_1(\min(P_i^{LF}(k) - P_i^L(k), 0))^2$

where $P_i^{LF}$ represents the satisfactory load level and $\alpha_l$ is a positive constant. Daily load characteristics can be obtained in real time using short-term electric power demand forecasting methods [16]. The above cost function is nonzero only when there is load shedding, i.e., when $P_i^L(k) > P_i^{LF}(k)$.

The system's energy recovery can be modeled using an exponential smoothing method, which is designed to utilize the forecast error from the previous period to correct and improve the prediction for the current period. In equation form:

$$P_i^{RES}(k+1) = P_i^{RES}(k) + \alpha_r \left(P_i^r(k) - P_i^{RES}(k)\right),$$

(12) $\underline{P_i^{RES}} \le P_i^{RES}(K) \le \overline{P}_i^{RES}$

where $P_i^{RES}(k)$ is the forecasted power generated by the i-th source, $\alpha_r$ is a smoothing constant ($0<\alpha_r<1$), $P_i^r(k)$ is the actual active power during period k, and $P_i^{RES}$ and $P^-_i{}^{RES}$ are the minimum and maximum power output of the source, respectively.

4. **Power Balance:** It is assumed that all microgrid loads are in islanded mode. In collaborative microgrid systems, supply and demand balance is achieved not only within the local microgrid—where power is generated from DGs and storage—but also in neighboring systems that have surplus energy. Therefore, the following equality constraints are maintained for the electrical components:

(13) $P_i^b(k) = P_i^s(k) + P_{ij}(k) + P_i^C(k)$

(14) $P_i^s(k) = P_i^{RES}(k) - P_i^L(k)$

(15) $P_{ij}(k) = \sum_{j \neq i} a_{ij} P_j^S(k)$

(16) $P_{ij}(k) \geq 0$

Note that the power exchanged with the storage, $P_i^b(k)$, at each time interval depends on the energy mismatch $P_i^s(k)$, the controllable generation $P_i^C(k)$, and the excess power from other microgrids $P_{ij}(k)$, scaled by the coordination factor $a_{ij}$ . Considering the priority of using power to meet local demand, $P_{ij}(k)$ is greater than or equal to zero.

**System Modeling:**

Based on the system dynamics in (1) and (6) and the power balance constraints in (8)–(10), the following subsystem model is obtained:

(17) $x_i(K+1) = M_i x_i(K) + Q_i u_i(K) + \sum_{j=1, j \neq i}^{m} A_{ij} x_j(k) + \sum_{j=1, j \neq i}^{m} B_{ij} u_j(k) + L_i w_i(k) \quad , i = 1, \ldots\ldots, m,$

which

$$x_i(K) = [(1/\eta_i) E_i(k) \quad P_i^{RES}(k) \quad P_i^C(k)]^T$$

$u_i(k) = [P_i^L(k)]$

$w_i(k) = [P_i^r(k)]$

$$M_i = \begin{bmatrix} 1 & 1 & 1 \\ 0 & 1-\alpha_{ri} & 0 \\ 0 & 0 & 1 \end{bmatrix}, Q_i = \begin{bmatrix} -1 \\ 0 \\ 0 \end{bmatrix},$$

$$A_{ij} = \begin{bmatrix} 0 & a_{ij} & 0 \\ 0 & 0 & 0 \\ 0 & 0 & 0 \end{bmatrix}, B_{ij} = \begin{bmatrix} -a_{ij} \\ 0 \\ 0 \end{bmatrix},$$

$$L_i = \begin{bmatrix} 0 \\ \alpha_{ri} \\ 0 \end{bmatrix}, \quad i, j = 1, \ldots, m$$

Here, $x_i(k)$ represents the states of subsystem i, $u_i(k)$ is the input of subsystem i, and $w_i(k)$ denotes the external inputs from other subsystems that affect subsystem iii at sampling step k. The matrices $M_i$ , $Q_i$ , and $L_i$ are the corresponding state-space matrices.

**Stability of Multi-Microgrid Systems**

**Definition 1.** The system in (13) is stable if, for all finite x(k), there exists a finite quadratic Lyapunov function V(k) such that:

(18) $\Delta V(k) := V(k+1) - V(k) < 0$

**Theorem 1.** The augmented system in (13) is stable if a state-feedback control law exists.

(19) $\overline{u}(k+n|k) = -(B^T P B + S_1)^{-1}((B^T P A - S_2)\overline{x}(k+n|k) - S_5^T)$

and the following optimization problem can be solved subject to the LMI constraints:

(20) $\min_{\gamma, Q} \gamma$

Algorithm 2. Hypothetical Distributed MPC

1. Initialize the values $E_i(0), P_i^{RES}(0), P_i^C(0), P_i^L(0), P_i^s(0), \forall i = 1, \dots, m.$
2. Execute for k=1:
3. Measure $P_i^{RES}(k)$ from the previous iteration and set $x_i(k|k) = x_i(k)$
4. Take a measurement of the state $E_i(k)$ to decide whether to charge or discharge the energy.
5. Solve the optimization problem.
6. Send $\hat{P}_i^s(k)$ to the neighboring agents j, collect $P^{\wedge}{}_j^s(k)$ from them, and proceed to Step 5.
7. Continue until convergence is achieved.
8. Execute the optimal control action for $u_i^*(k)$
9. $k \leftarrow k + 1$ And proceed to Step 3.
10. End for.

Considering

$$)21\ (\begin{bmatrix} -\gamma & \overline{x}^T(k) \\ * & -Q \end{bmatrix} < 0$$

$$)22\ (\begin{bmatrix} -Q & \Delta_{12} & \Delta_{13} & \Delta_{14} & \\ * & -S_5 S_1^{-1} S_5^T & (BS_1^{-1}S_5^T)^T & 0 \\ * & * & -Q - BS_1^{-1}B^T & 0 \\ * & * & * & -I \end{bmatrix}$$

$$)23\ (\begin{bmatrix} -S_3 & S_2^T \\ S_2 & -S_1 \end{bmatrix} < 0$$

where the symbol * denotes a symmetric structure, and I is an identity matrix of appropriate dimension,$Q \succ 0, S_1 \succ 0, S_2, S_3 \succ 0, S_4, S_5$ the variables are matrices of appropriate dimensions.$S_6$ The variable is a positive scalar. $\gamma > 0$ and:

$$\Delta_{12} = -QS_2^T S_1^{-1} S_5^T - QS_4^T$$

$$\Delta_{13} = Q(A| + BS_1^{-1}S_2)^T$$

$$\Delta_{14} = Q(S_3 - S_2^T S_1^{-1} S_2)^{1/2}$$

$$Q = P^{-1}, \quad e = \alpha_b \overline{E}, \quad f_i(k) = P_i^{Lf}(k)$$

$l_r = [0 \quad 1 \quad 0], \quad l_b = [\eta_i \quad 0 \quad 0]$

$$S_1 = \begin{bmatrix} \xi_r + \xi_L & & \\ & \ddots & \\ & & \xi_r + \xi_L \end{bmatrix}$$

$$S_2 = \begin{bmatrix} \xi_r \xi_L & & \\ & \ddots & \\ & & \xi_r \xi_L \end{bmatrix}$$

$$S_3 = \begin{bmatrix} l_r^T \xi_r l_r + l_b^T \xi_b l_b & & \\ & \ddots & \\ & & l_r^T \xi_r l_r + l_b^T \xi_b l_b \end{bmatrix}$$

$$S_4 = [e\xi_b l_b \quad \dots \quad e\xi_b l_b]$$

$$S_5 = [f_1(k)\xi_b \quad \dots \quad f_m(k)\xi_L]$$

$$S_6 = me^2\xi_b + \sum_{i=1}^{m}(f_i^2(k)\xi_L)$$

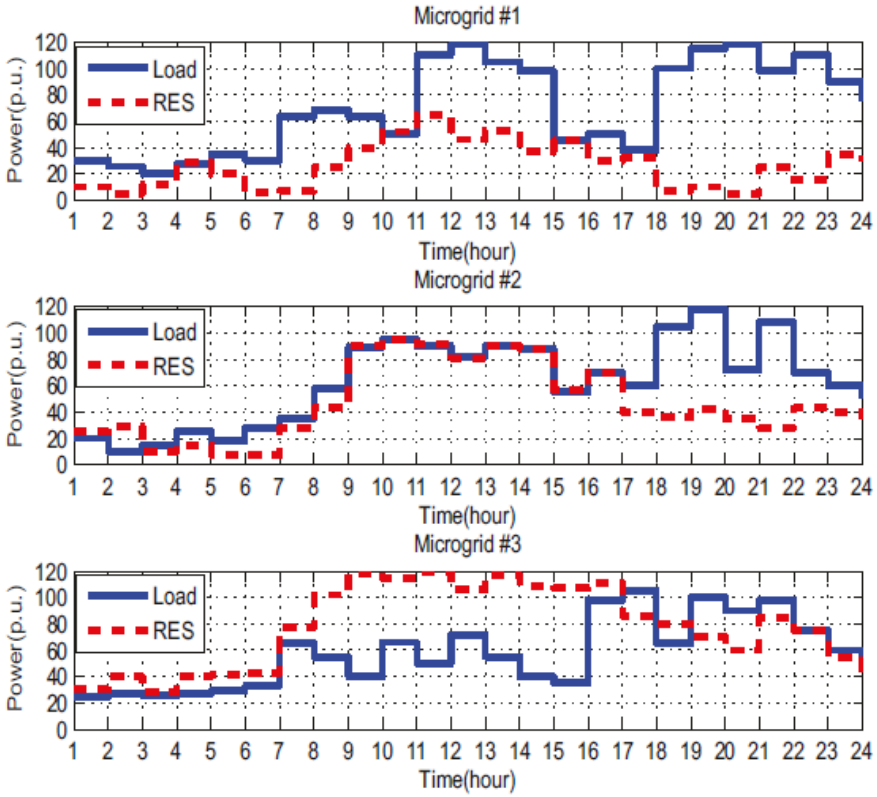


Figure 17: Daily demand and power generated by HVAC energy sources.

The power generated in Microgrid #1 is less than the demand from 7 a.m. to 7 p.m., while the energy in Microgrid #2 is approximately equal to its demand, and the generation in Microgrid #3 exceeds its demand. To compensate for the mismatch between demand and RES, the microgrid systems require coordination through energy exchange. The forecasted curves are shown with red dashed lines, while the actual profiles are represented by solid blue lines. It can be observed that the predicted energy generation closely follows the actual values at each time step.

**Conclusion**

This study employed two evaluation metrics, RMSE and $R^2$, to compare prediction methods. RMSE represents an average of prediction errors; it remains low when most errors are small and only a few are large. The $R^2$coefficient indicates the proportion of variance in the predicted values that aligns with the variance of the actual values. Consequently, $R_2$can be significantly affected by large errors, as it measures how well the predicted values fit the actual data.

The study applied both the MLP and Genetic Algorithm methods to assess their effectiveness in time-series prediction. Based on the $R^2$results for predicting room temperature and humidity under an HVAC system, the Genetic Algorithm did not show a significant improvement over the MLP method. One notable advantage of the Genetic Algorithm is related to the MLP network's data preparation: the entire dataset was randomly

shuffled, with 75% used for training and 25% for testing, which may have influenced the results.

Analysis of prediction accuracy for both temperature and humidity revealed that the MLP network achieved the highest precision. The Genetic Algorithm performed poorly in predicting humidity, which was further confirmed by evaluating the MLP network without shuffling the data. In this scenario, $R^2$=0.559and RMSE = 0.12. The substantial decrease in $R^2$compared to the shuffled-data MLP case, alongside the low $R_2$of the Genetic Algorithm, underscores the superior performance of MLP for these predictions.

Finally, the results suggest further research into using solar energy as an alternative power source for HVAC systems, evaluating potential operational cost reductions, and simulating HVAC performance using existing software, with comparisons drawn to the findings of this study.

**References:**

1. Mirakhorli, A. and B. Dong, *Market and Behavior driven Predictive Energy Management for Residential Buildings.* Sustainable Cities and Society, 2018. **38.**
2. Chen, C., et al., *MPC-Based Appliance Scheduling for Residential Building Energy Management Controller.* Smart Grid, IEEE Transactions on, 2013. **4**: p. 1401-1410**.**
3. Aftab, M., et al., *Automatic HVAC control with real-time occupancy recognition and simulation-guided model predictive control in low-cost embedded system.* Energy and Buildings, 2017. **154 :**p. 141-156
4. Aghileh, A., Modeling and Control of an HVAC System in a Residential Building for Energy Consumption Reduction, in the 27th Annual International Conference of the Iranian Society of Mechanical Engineers, 2019.Gholamzadehmir, M., et al., *Adaptive-predictive control strategy for HVAC systems in smart buildings – A review.* Sustainable Cities and Society, 2020. **63**: p. 102480**.**
5. Carli, R., et al. *IoT Based Architecture for Model Predictive Control of HVAC Systems in Smart Buildings*. Sensors, 2020. **20**, DOI: 10.3390/s20030781**.**
6. Lymperopoulos, G. and P. Ioannou, *Building temperature regulation in a multi-zone HVAC system using distributed adaptive control.* Energy and Buildings, 2020. **215**: p**.109825 .**
7. Esrafilian-Najafabadi, M. and F. Haghighat, *Occupancy-based HVAC control systems in buildings: A state-of-the-art review.* Building and Environment, 2021. **197**: p. 107810**.**
8. Taheri, S., P. Hosseini, and A. Razban, *Model predictive control of heating, ventilation, and air conditioning (HVAC) systems: A state-of-the-art review.* Journal of Building Engineering, 2022. **60**: p. 105067**.**
9. Nadeem, T., et al., *Designing of Heating, Ventilation, and Air Conditioning (HVAC) System for Workshop Building in Hot and Humid Climatic Zone Using CLTD Method and HAP Analysis: A Comparison.* Arabian Journal for Science and Engineering, 2022. **47.**
10. Bohara, B., et al., *Experimental Study of the Model Predictive Control for a Residential Split Air Conditioner.* e-Prime - Advances in Electrical Engineering, Electronics and Energy, 2023. **3**: p. 100099**.**
11. Pham, V. and V. Nguyen, *A study on optimization of HVAC system in buildings using gray wolf optimizer (GWO) and artificial neural network (ANN).* Asian Journal of Civil Engineering, 2023. **24**: p. 1-15**.**
12. Faddel, S., *Modeling and Robust Optimization of Commercial Air-Water HVAC System.* IEEE Transactions on Industry Applications, 2023. **PP**: p. 1-10**.**
13. Zhao, D., et al., *Data-driven online energy management framework for HVAC systems: An experimental study.* Applied Energy, 2023. **352**: p. 121921**.**

14. Pandey, B., et al., *A thermal comfort-driven model predictive controller for residential split air conditioner.* Journal of Building Engineering, 2021. **42**: p. 102513**.**
15. Shtovba, S., *Ant Algorithms: Theory and Applications.* Programming and Computer Software, 2005. **31**: p. 167-178**.**